
Monotone Optimisation with Learned Projections

Ahmed Rashwan¹ Keith Briggs² Chris Budd¹ Lisa Kreusser³

Abstract

Monotone optimisation problems admit specialised global solvers such as the *Polyblock Outer Approximation* (POA) algorithm, but these methods typically require explicit objective and constraint functions. In many applications, these functions are only available through data, making POA difficult to apply directly. We introduce an algorithm-aware learning approach that integrates learned models into POA by directly predicting its projection primitive via the *radial inverse*, avoiding the costly bisection procedure used in standard POA. We propose Homogeneous–Monotone Radial Inverse (HM-RI) networks, structured neural architectures that enforce key monotonicity and homogeneity properties, enabling fast projection estimation. We provide a theoretical characterisation of radial inverse functions and show that, under mild structural conditions, a HM-RI predictor corresponds to the radial inverse of a valid set of monotone constraints. To reduce training overhead, we further develop relaxed monotonicity conditions that remain compatible with POA. Across multiple monotone optimisation benchmarks (indefinite quadratic programming, multiplicative programming, and transmit power optimisation), our approach yields substantial speed-ups in comparison to direct function estimation while maintaining strong solution quality, outperforming baselines that do not exploit monotonic structure.

1. Introduction

Many optimisation problems in modern machine learning pipelines involve objectives or constraints that are not analytically available and must instead be inferred from data (Fajemisin et al., 2024). Prominent examples include learned surrogate objectives in model-free optimisation (Jeon et al., 2019; Lin et al., 2021) and regularisers

learned through bilevel training for inverse problems (Herrtrich et al., 2025; Zou et al., 2023). In practice, such problems are most often addressed using local search methods (Tong et al., 2025; Perakis & Tsiourvas, 2022). While these approaches scale well, they provide no guarantees of global optimality and are highly sensitive to the non-convexity introduced by learned components. At the opposite extreme, optimisation problems involving neural networks can often be cast as mixed-integer linear programs (MILPs) (Fischetti & Jo, 2018), enabling exact global optimisation but at prohibitive computational cost and with poor scaling in network size. These two extremes highlight a central challenge: how to integrate learned components into optimisation algorithms in a principled and reliable manner, particularly when the optimiser relies on structural assumptions that generic learned models do not satisfy.

A particularly powerful structural assumption is monotonicity: a function is monotone if it is non-decreasing (or non-increasing) in each input. Monotonicity arises naturally in applications such as resource allocation, communications (Y. J. Zhang et al., 2013), and computer simulations (Golchi et al., 2015), and it enables specialised global optimisation methods for otherwise difficult non-convex problems (Konno et al., 2013; Tuy, 2000). Monotone optimisation algorithms have been especially successful in communication network design (Jorswieck & Larsson, 2010; Utschick & Brehmer, 2011), yet they remain underexplored in learning-based pipelines, where objectives and constraints are only available through data.

The primary method for global monotone optimisation is the *Polyblock Outer Approximation* (POA) algorithm (Tuy et al., 2005). POA is a branch-and-bound-style procedure that exploits monotonicity to iteratively refine a rectangular approximation of the feasible region, systematically converging to the global optimum. POA is attractive because it is broadly applicable and relies on a small number of highly structured internal operations, most notably a repeated monotone projection step. Crucially, in many practical problems monotonicity is known from domain knowledge even when the underlying functions are unknown or expensive to evaluate, making POA a natural candidate for data-driven global optimisation. This suggests an algorithm-aware learning approach (Fang et al., 2024), in which learned components are designed to inter-

¹University of Bath ²BT Research ³Monumo. Correspondence to: Ahmed Rashwan <ar3009@bath.ac.uk>.

face directly with POA’s core operations while preserving the assumptions required for correctness.

We observe that POA does not require explicit access to the monotone constraint functions themselves. Instead, it only uses a projection subroutine, typically implemented via a bisection-based feasibility search. We make this dependency explicit by identifying the associated *radial inverse* as the fundamental object required by POA, and show that estimating this map is sufficient to run the algorithm effectively. This shifts learning away from approximating constraint functions directly and toward approximating the internal primitive that POA actually uses, enabling tighter algorithmic integration and avoiding unnecessary modelling burden.

Since POA relies on monotonic structure, learned surrogates should preserve monotonicity, whether they estimate the radial inverse directly or approximate monotone constraint functions. Classical monotone interpolation techniques are computationally expensive and scale poorly with dataset size (Beliakov, 2005). Neural networks provide scalable alternatives: some neural architectures enforce monotonicity by construction, including *Deep Lattice Networks* (You et al., 2017), *Min–Max Networks* (Daniels & Velikova, 2010), and constrained monotone architectures (Runje & Shankaranarayana, 2023), but these designs can be restrictive or hard to scale to high-dimensional settings. A complementary regularisation-based line of work verifies monotonicity post hoc; notably, *Certified Monotone Networks* (Liu et al., 2020) use MILPs to certify monotonicity of ReLU feed-forward networks. Our work follows this verification-oriented perspective, but aims increase robustness by adopting relaxed monotonicity conditions.

Building on this, we propose Homogeneous–Monotone Radial Inverse (HM-RI) networks, a structured neural architecture tailored specifically for radial inverse estimation. HM-RI networks enforce the structural properties required by POA, most importantly positive-homogeneity and monotonicity, while remaining efficient to train through relaxed certified monotone components. Beyond the architecture, we give a theoretical characterisation of radial inverse functions via a small set of natural properties, and show that HM-RI networks satisfy these properties under mild conditions. Consequently, the learned models are directly compatible with POA, ensuring correct integration while delivering substantial computational speed-ups in practice.

We evaluate our approaches on four classes of monotone optimisation problems (indefinite quadratic programming, multiplicative programming, and two transmit power optimisation problems), demonstrating that POA can be effectively deployed with learned components. Radial inverse estimation provides up to a $5\times$ speed-up compared to direct

estimation of monotone surrogates, while producing solutions that are often empirically near-global optima. These approaches also consistently outperform local optimisation baselines which do not leverage monotonic structure.

1.1. Contributions

- We develop an algorithm-aware learning framework for integrating learned constraint models into the Polyblock Outer Approximation (POA) algorithm for monotone optimisation.
- We introduce a relaxation of certified monotone networks that reduces training cost and improves empirical performance, particularly for learning monotone functions with flat or piecewise-constant structure.
- We introduce radial inverse functions as a constraint representation and learning target for POA, and provide sufficient conditions under which a learned map corresponds to the radial inverse of an increasing function, ensuring compatibility with POA.
- We propose Homogeneous–Monotone Radial Inverse (HM-RI) networks, a structured architecture for radial inverse estimation, which removes the bisection-based feasibility search in each POA iteration.
- We introduce several simplified variants of HM-RI that remove architectural components while retaining strong empirical performance, clarifying which design choices matter in practice.
- We evaluate our methods on multiple classes of monotone optimisation problems and show that POA with learned components achieves accurate, often near-optimal solutions in practice, while substantially reducing optimisation runtime relative to bisection-based POA.

2. Preliminaries

2.1. Monotone optimisation

We begin with basic notation. For $n \in \mathbb{N}$, let $[n] := \{1, \dots, n\}$. We write $\mathbb{R}_+ := [0, \infty)$. For vectors $x, y \in \mathbb{R}^n$, we use the standard product order: $x \leq y$ (resp. $x < y$) if $x_i \leq y_i$ (resp. $x_i < y_i$) for all $i \in [n]$. We write $x \not\leq y$ to denote the negation of $x < y$, i.e., there exists $i \in [n]$ such that $x_i \geq y_i$. Given $x \leq y$, define the (closed) axis-aligned box

$$[x, y] := \prod_{i=1}^n [x_i, y_i],$$

with open boxes defined analogously.

A function $f : \mathbb{R}_+^n \rightarrow \mathbb{R}$ is (*strictly*) *increasing* if $f(x) \leq f(y)$ (resp. $f(x) < f(y)$) whenever $x \leq y$ (resp. $x < y$). It

is (*strictly*) *decreasing* if $-f$ is (*strictly*) increasing. We say that f (*strictly*) *monotone* if it is either (*strictly*) increasing or (*strictly*) decreasing.

We consider monotone optimisation problems of the form

$$\begin{aligned} \max_{x \in \mathbb{R}_+^n} \quad & f(x) \\ \text{s.t.} \quad & g_i(x) \leq u_i, \quad i \in [m_g], \\ & h_j(x) \geq l_j, \quad j \in [m_h], \end{aligned} \quad (2.1)$$

where f , $\{g_i\}_{i=1}^{m_g}$, and $\{h_j\}_{j=1}^{m_h}$ are increasing functions on \mathbb{R}_+^n , and $u_1, \dots, u_{m_g}, l_1, \dots, l_{m_h} \in \mathbb{R}$. Let

$$\begin{aligned} \mathcal{G} &:= \{x \in \mathbb{R}_+^n : g_i(x) \leq u_i, i \in [m_g]\}, \\ \mathcal{H} &:= \{x \in \mathbb{R}_+^n : h_j(x) \geq l_j, j \in [m_h]\}, \end{aligned} \quad (2.2)$$

so that the feasible set is $\mathcal{F} := \mathcal{G} \cap \mathcal{H}$, which we assume is non-empty and that \mathcal{G} is compact (e.g., by restricting x to a bounded box $[0, b] \subset \mathbb{R}_+^n$).

2.2. Polyblocks and outer approximation

Rectangles and polyblocks. For any $x \in \mathbb{R}_+^n$, define the associated *rectangle*

$$P_x := [0, x] := \prod_{i=1}^n [0, x_i].$$

For a set $S \subseteq \mathbb{R}_+^n$, define its induced *rectangular hull*

$$P_S := \bigcup_{s \in S} P_s.$$

Intuitively, P_S is the set of all points dominated by some $s \in S$. A *polyblock* is a rectangular hull generated by a finite set V , i.e. a set of the form P_V for finite $V \subset \mathbb{R}_+^n$.

A set $S \subset \mathbb{R}_+^n$ is said to be *normal* if $P_S = S$ or, equivalently, if $x \in S$ and $0 \leq y \leq x$ implies $y \in S$. By monotonicity of the constraint functions, the sets \mathcal{G} and \mathcal{H}^c are normal.

Monotone projection. For a normal set $S \subseteq \mathbb{R}_+^n$ and $x \in \mathbb{R}_+^n$, define the *monotone projection* of x onto S by

$$\pi_S(x) := \alpha_S(x)x, \quad \alpha_S(x) := \sup\{\alpha \in \mathbb{R}_+ : \alpha x \in S\}.$$

Equivalently, $\pi_S(x)$ is the largest point on the ray $\{rx : r \geq 0\}$ that lies in S .

Polyblock Outer Approximation (POA). The Polyblock Outer Approximation (POA) algorithm solves (2.1) by constructing a nested sequence of polyblock supersets of the feasible region:

$$P_{V^0} \supseteq P_{V^1} \supseteq \dots \supseteq \mathcal{F},$$

where each $V^t \subset \mathbb{R}_+^n$ is a finite set of vertices. Since f is increasing, its maximum over a polyblock is attained at one of the vertices:

$$\hat{x}^t \in \arg \max_{x \in V^t} f(x) \subset \arg \max_{x \in P_{V^t}} f(x). \quad (2.3)$$

Thus $f(\hat{x}^t)$ provides an upper bound on the optimal value $f^* := \max_{x \in \mathcal{F}} f(x)$. POA refines V^t while maintaining this upper bound and feasible candidates obtained via projection.

POA is initialized with a dominant vertex $b \in \mathbb{R}_+^n$ such that $\mathcal{F} \subseteq P_b$, and sets $V^0 := \{b\}$. At iteration $t \geq 0$, it computes the current maximizer \hat{x}^t from (2.3) using V^t , and projects it onto \mathcal{G} via the monotone projection $z^t := \pi_{\mathcal{G}}(\hat{x}^t)$, defined in Section 2.2.

When $\{g_i\}$ are known, $\pi_{\mathcal{G}}(\hat{x}^t)$ can be computed by bisection along the ray $\{r\hat{x}^t : r \geq 0\}$, see Appendix B.1.

By maximality of the projection, no point strictly larger than z^t (componentwise) can lie in \mathcal{G} , so the region $(z^t, \infty) := \{x \in \mathbb{R}_+^n : x > z^t\}$ can be removed from the current polyblock without excluding any feasible points, yielding a refined polyblock. The corresponding vertex set \hat{V}^{t+1} is obtained by taking V^t and replacing each vertex $s \in V^t$ with $s > z^t$ by n new vertices. Each new vertex is formed by reducing one coordinate of s to match the corresponding coordinate of z^t , while keeping all other coordinates fixed. Finally, since \mathcal{H}^c is normal, any vertex $s \notin \mathcal{H}$ can be discarded since its corresponding rectangle $P_s \subset \mathcal{H}^c$ does not intersect \mathcal{F} . This yields the updated vertex set

$$V^{t+1} := \hat{V}^{t+1} \cap \mathcal{H}.$$

We then update $\hat{x}^{t+1} \in \arg \max_{x \in V^{t+1}} f(x)$ and iterate until a stopping criterion is reached. The construction of the vertex sets V^0, V^1 and V^2 is illustrated in Figure 1. Full details are given in Appendix B.

2.3. Learning monotone constraints

Learned objective and constraints. We study problems of the form (2.1) in which any subset of the functions $\{f, g_1, \dots, g_{m_g}, h_1, \dots, h_{m_h}\}$ are represented by learned surrogates, which may approximate the functions directly or some derived quantity sufficient for optimisation. Such models may be trained offline (supervised or self-supervised) or updated online during the optimisation procedure. Throughout, we assume only that the optimisation algorithm has oracle access to any learned models, i.e. it can evaluate them at arbitrary inputs.

While the construction applies in principle to any learned component (objective or constraints), we focus primarily on learning the upper-bound constraints $\{g_i\}_{i \in [m_g]}$, since they are queried most frequently by POA and admit addi-

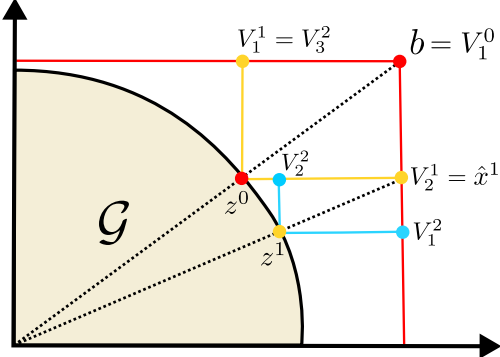


Figure 1. Illustration of the construction of $V^0 = \{b\}$, $V^1 = \{V_1^1, V_2^1\}$ and $V^2 = \{V_1^2, V_2^2, V_3^2\}$ of POA in 2D with $m_h = 0$, i.e., $\mathcal{H} = \mathbb{R}_+^2$. Points are color coded by iteration. Vertices are indexed by subscripts.

tional structure exploited by our radial inverse approximation (Section 3).

Certified monotone networks. To preserve the monotone structure required by POA (Section 2.2) and by the feasible-set geometry (Sections 2.1), the learned surrogates should be monotone. Beyond correctness, monotonicity also serves as a useful inductive bias, improving generalisation in supervised learning (Runje & Shankaranarayana, 2023).

We will be building on *Certified Monotone Networks* (Liu et al., 2020), which enforce monotonicity for feed-forward ReLU networks $g_\theta : \mathbb{R}_+^n \rightarrow \mathbb{R}$ trained with arbitrary loss functions. During training, monotonicity is encouraged via a regulariser which penalises sufficiently small gradients:

$$R(\theta) = -c \mathbb{E}_{x \sim P_b} \left[\sum_{j \in [n]} \min\{\partial_{x_j} g_\theta(x), \eta\} \right], \quad (2.4)$$

where $\eta \geq 0$ is the minimum permitted gradient and $c > 0$ is the regularisation strength. This expectation is estimated using points sampled uniformly from P_b . In practice, successful certification typically requires $\eta > 0$.

After training, monotonicity can be *certified* by solving a MILP to verify that $\partial_{x_j} g_\theta(x) \geq 0$ for all $j \in [n]$ over the relevant domain (e.g. $x \in P_b$ for the initialisation of POA). If certification fails, one increases c and retrains until certification succeeds.

For deeper networks, certification can be applied layer-wise: monotonicity is enforced for each consecutive layer pair, and the overall network remains monotone by closure under composition.

3. Estimating projections using learned radial inverse functions

While POA needs direct oracle access to the objective f and lower-bound constraints $\{h_i\}_{i \in [m_h]}$, it interacts with the upper-bound constraints $\{g_i\}_{i \in [m_g]}$ only through the monotone projection π_G (defined in Section 2.2). A direct implementation computes $\pi_G(x)$ by bisection along the ray $\{rx : r \geq 0\}$, repeatedly evaluating the constraints. In our experiments, this inner bisection loop constitutes the dominant computational cost, particularly when the constraints are represented by large surrogate models. This motivates learning the projection map itself, rather than first learning the constraint functions and then performing bisection at inference time. It also avoids bisection failures when a learned constraint model is only approximately monotone.

To enable this, we introduce the *radial inverse* as an explicit learning target for approximating π_G . The radial inverse captures the ray-based scaling required for feasibility and yields closed-form projection estimates, allowing POA to be deployed with learned projection primitives.

3.1. Radial inverse function

Let $g : \mathbb{R}_+^n \rightarrow \mathbb{R}$ be an increasing function. We define its *radial inverse* $\rho_g : \mathbb{R}_+^n \times \mathbb{R} \rightarrow \mathbb{R}_+ \cup \{\infty\}$ as

$$\rho_g(x, y) := \inf\{r > 0 : g(x/r) \leq y\}, \quad (3.1)$$

with the convention $\inf \emptyset = \infty$, implying that $\rho_g(x, y) \in [0, \infty]$. Let $K(y) := \{u \in \mathbb{R}_+^n : g(u) \leq y\}$ denote the sub-level set of g at level y . Then ρ_g coincides with the *gauge* of $K(y)$:

$$\rho_g(x, y) = \gamma_{K(y)}(x), \quad (3.2)$$

where $\gamma_S(x) := \inf\{r > 0 : x \in rS\}$ is the gauge function for a set $S \subset \mathbb{R}_+^n$ (Schaefer & Wolff, 1999). Intuitively, $\rho_g(x, y)$ is the smallest radial scaling needed so that x/r becomes feasible for the sub-level constraint $g(\cdot) \leq y$.

We collect basic properties of ρ_g for increasing g :

Proposition 1 (Radial inverse properties). *Let $g : \mathbb{R}_+^n \rightarrow \mathbb{R}$ be an increasing function, and let $x, x' \in \mathbb{R}_+^n$ and $y, y' \in \mathbb{R}$. Then ρ_g satisfies:*

(i) **(Positive-homogeneity in x)** For all $\alpha > 0$,

$$\rho_g(\alpha x, y) = \alpha \rho_g(x, y).$$

(ii) **(Monotonicity)** $\rho_g(x, y)$ is increasing in x and decreasing in y : If $x \leq x'$ then $\rho_g(x, y) \leq \rho_g(x', y)$; if $y \leq y'$ then $\rho_g(x, y') \leq \rho_g(x, y)$.

(iii) **(Right-continuity in y)** For any x and y ,

$$\lim_{\epsilon \downarrow 0} \rho_g(x, y + \epsilon) = \rho_g(x, y).$$

(iv) **(Well-posedness)** For all $x \in \mathbb{R}_+^n$, there exists $y, y' \in \mathbb{R}$ with $y > y'$ such that

$$\rho_g(x, y) \leq 1, \text{ and } \rho_g(x, y') > 1. \quad (3.3)$$

The proof of Proposition 1 is provided in Appendix A.1.

3.2. From radial inverse functions to monotone projections

We first show that monotone projections onto a normal set admit a closed-form expression in terms of the radial inverses of the individual constraints.

Proposition 2 (Projection via radial inverses). *Let \mathcal{G} be a compact normal set as defined in (2.2). Then, for any $x \in \mathbb{R}_+^n$, the monotone projection $\pi_{\mathcal{G}}$ satisfies*

$$\pi_{\mathcal{G}}(x) = \left(\max_{i \in [m_g]} \rho_{g_i}(x, u_i) \right)^{-1} x,$$

For each constraint function $g_i(x)$, we propose to learn its radial inverse with a network ϕ_{θ_i} , i.e., $\rho_{g_i}(x, y) \approx \phi_{\theta_i}(x, y)$. By Proposition 2, this yields the approximation

$$\pi_{\mathcal{G}}(x) \approx \left(\max_{i \in [m_g]} \phi_{\theta_i}(x, u_i) \right)^{-1} x.$$

Importantly, Proposition 2 accesses each radial inverse only through its evaluation at the threshold u_i . As a result, a single learned surrogate $\phi_{\theta_i}(x, y)$ can be reused for any choice of u_i without retraining, enabling flexible deployment across problem instances.

Approximating ρ_{g_i} with a learned map ϕ_{θ_i} naturally raises the question of when such a map can be interpreted as the radial inverse of a monotone function. The following result shows that the structural properties listed in Proposition 1 are sufficient to characterise radial inverse functions.

Proposition 3. *Let $h : \mathbb{R}_+^n \times \mathbb{R} \rightarrow \mathbb{R}_+ \cup \{\infty\}$ satisfy properties (i)–(iv) in Proposition 1 for all $(x, y) \in \mathbb{R}_+^n \times \mathbb{R}$. Then there exists an increasing function $g : \mathbb{R}_+^n \rightarrow \mathbb{R}$ such that $h = \rho_g$.*

Proposition 3 motivates our architectural choices: by enforcing properties (i)–(iv), we restrict the learned model ϕ to the class of valid radial inverses. Consequently, the learned projection primitive remains compatible with POA even without explicitly recovering the underlying constraint functions. Proofs of Propositions 2 and 3 are provided in Appendix A.2.

4. Structured models for radial inverse estimation

In this section, we introduce the HM-RI neural network architecture ϕ_{θ} , designed to estimate the radial inverse used

by POA while satisfying properties (i)–(iv) in Proposition 1. We begin by describing the relaxed certified monotonicity method that underpins our approach. We then present the HM-RI architecture and training details, before introducing simplified architectures.

4.1. Relaxed certified monotone networks

While certified monotone networks provide exact monotonicity guarantees, they can be challenging to deploy in practice. Since small positive gradients are penalised ($\eta > 0$ in (2.4)), it is difficult to learn functions which are not *strictly* monotone. Moreover, the network g_{θ} often converges to a state that is monotone over almost all of P_b , with violations confined to very small ReLU affine regions. In such cases, certification may fail even though the regulariser (2.4) is effectively inactive in practice, as sampled gradients almost surely exceed η . To address this, introduce *relaxed certified networks*, which trade exact monotonicity for improved optimisation and empirical performance.

Our relaxation has two components. First, to handle the problem of small affine regions, we ignore regions below a minimum size τ when enforcing monotonicity. This substantially reduces the cost of certification by omitting tiny regions that have negligible impact on overall monotone behaviour but are difficult to constrain through regularisation. Second, to address the difficulty of learning functions which are not strictly monotone everywhere, we allow a small controlled violation of monotonicity by permitting gradients to be slightly negative up to a fixed tolerance, i.e. $\partial_{x_j} g_{\theta}(x) \geq -\delta$ for a user-specified tolerance $\delta \geq 0$. This allows us to set $\eta = 0$, which improves estimation of functions with flat or gently increasing regions.

Although these relaxations remove formal monotonicity guarantees, the models largely retain the desired monotone behaviour in practice and consistently lead to improved test performance in our experiments. Exact definitions and implementation details are provided in Appendix C. We also include ablation experiments which demonstrate the benefits of each relaxation in Appendix E.2.

4.2. Homogeneous-monotone radial inverse (HM-RI) networks

The aim of this section is to design a neural architecture which satisfies the structural properties in Proposition 1. Continuity (iii) holds for feed-forward networks with continuous activations. We therefore focus on enforcing positive homogeneity (i) and monotonicity (ii), and on partially promoting the well-posedness requirement (iv) via a our training objective.

We construct a scalar-valued model $\phi_{\theta_i}(x, y)$ that is monotone in y , and both monotone and positive-homogeneous in

x. Specifically, we define

$$\phi_{\theta_i}(x, y) = \tanh(\sigma_{\theta_i}(y))^\top \psi_{\theta_i}(x),$$

where $\sigma_{\theta_i} : \mathbb{R} \rightarrow \mathbb{R}^w$ and $\psi_{\theta_i} : \mathbb{R}_+^n \rightarrow \mathbb{R}^w$ are feed-forward networks and $\tanh(\cdot)$ is applied element-wise.

If σ_{θ_i} and ψ_{θ_i} are element-wise monotone and ψ_{θ_i} is positive-homogeneous, then ϕ_{θ_i} inherits the desired monotonicity and homogeneity properties. To achieve monotonicity, we train both subnetworks as relaxed certified monotone networks. To enforce positive-homogeneity, we construct ψ_{θ_i} using bias-free linear layers with ReLU activations, which are themselves positively homogeneous. Such bias-free networks are universal approximators of positive-homogeneous functions (Bamberger et al., 2025).

Finally, regarding well-posedness (iv), we observe that the condition is typically satisfied in practice. Even when it fails, a relaxed form of Proposition 3 can still be established; see Appendix A.2.

4.2.1. TRAINING OBJECTIVE

The training procedure for the radial inverse surrogate ϕ_{θ_i} depends on the application. For our experiments, we consider a supervised setting in which ϕ_{θ_i} is trained on a dataset $\mathcal{D}_i = \{(x_j, y_j)\}_j$ satisfying $g_i(x_j) = y_j$.

For each training pair (x, y) , the definition of the radial inverse implies $\rho_{g_i}(x, y) \leq 1$, since taking $r = 1$ already reaches level y along the ray. We therefore train ϕ_{θ_i} to produce values close to 1 on the training data, while penalising overestimation more strongly in order to encourage the per-sample feasibility constraint $\phi_{\theta_i}(x, y) \leq 1$. This also helps enforce the upper-bound condition as required by the well-posedness property. We achieve this using an asymmetric squared loss,

$$L(\theta_i) = \sum_{(x, y) \in \mathcal{D}_i} \left(\mathcal{E}_{\theta_i}(x, y)^2 + \beta [\mathcal{E}_{\theta_i}(x, y)^+]^2 \right), \quad (4.1)$$

where $\mathcal{E}_{\theta_i}(x, y) = \phi_{\theta_i}(x, y) - 1$ and $(\cdot)^+ = \max(\cdot, 0)$. When $\phi_{\theta_i}(x, y) \leq 1$, this reduces to a standard least-squares loss. For $\phi_{\theta_i}(x, y) > 1$, the squared error is amplified by a factor of $1 + \beta$, placing additional penalty on violations of the constraint $\phi_{\theta_i}(x, y) \leq 1$.

When g_i is strictly monotone, the radial inverse satisfies $\rho_{g_i}(x, y) = 1$ for all samples, and the standard least-squares loss (corresponding to $\beta = 0$) is sufficient.

4.3. Simplified HM-RI models

In addition to HM-RI, we consider simplified variants obtained by relaxing one or both of its structural properties. Monotonicity is removed by replacing σ_θ and ψ_θ with standard feed-forward networks, while positive homogeneity is

relaxed by allowing bias terms in ψ_θ , eliminating the architectural guarantee of homogeneity. This yields three variants: H-RI (homogeneous only), M-RI (monotone only), and RI (neither property).

We find that variants without an architectural homogeneity guarantee do not yield meaningful projection estimates when trained using (4.1). To mitigate this, we encourage homogeneity through data augmentation. Specifically, for each $(x, y) \in \mathcal{D}$ we sample α uniformly from $[0.5, 2.5]$ and add the input pair $(\alpha x, y)$ with target value α to an augmented dataset. The error term in (4.1) is then replaced by $\mathcal{E}_{\theta_i}(\alpha x, y) = \phi_{\theta_i}(\alpha x, y) - \alpha$. Similar augmentation strategies have proven effective in other domains, such as computer vision (Shorten & Khoshgoftaar, 2019).

5. Application problems

We evaluate our approach on four families of monotone optimisation problems: indefinite quadratic programming, multiplicative programming, and two classes of transmit power optimisation problems. Across all experiments, the objective function is assumed known and the constraint set is learned from data. (Our relaxed certified monotone networks could also be applied to the objective or any lower-bound constraints, but we do not consider this setting here.)

Rather than learning a fixed finite collection of constraints $\{g_i\}_{i \in [m_g]}$, we learn parameterised families $\{g_z\}_{z \in \mathbb{R}^k}$ by treating z as an additional network input. Here, z collects the instance parameters (e.g., coefficients for quadratic and multiplicative constraints, or user locations for power control), so a single conditional model represents a continuum of constraints. We train neural approximations of either g_z directly, or of its radial inverse, using randomly generated samples (x, y, z) satisfying $g_z(x) = y$. This allows us to evaluate performance over diverse, randomly generated monotone optimisation instances, rather than a single fixed problem. We describe each family of problems and its corresponding constraint parametrisation below.

5.1. Indefinite quadratic programming

We consider problems of the form

$$\begin{aligned} \max_{x \in [0, 1]} \quad & x^T Q_0 x, \\ \text{s.t.} \quad & x^T Q_j x + c_j^T x \leq u_j, \quad j \in [m_g] \end{aligned} \quad (5.1)$$

where $Q_j \in \mathbb{R}_+^{n \times n}$, $c_j \in \mathbb{R}_+^n$, and $u_j \in \mathbb{R}_+$. The nonnegativity assumption ensures monotonicity; however, general polynomial problems can be transformed into monotone form (Tuy et al., 2005). Non-convex quadratic programs form a widely studied subclass of such problems (Park & Boyd, 2017). For the constraints in (5.1), the radial inverse is tractable since it reduces to solving a quadratic equation.

5.2. Multiplicative programming

We consider problems of the form

$$\begin{aligned} \max_{x \in [0,1]} \quad & x^T Q_0 x, \\ \text{s.t.} \quad & \prod_{i=1}^k (x^T Q_{i,j} x + c_{i,j}) \leq u_j, \quad j \in [m_g] \end{aligned}$$

where $Q_{i,j} \in \mathbb{R}_+^{n \times n}$, $c_{i,j} \in \mathbb{R}_+$, and $u_j \in \mathbb{R}_+$. Monotone optimisation has previously been applied successfully to related multiplicative programmes (Tuy & Luc, 2000). Unlike the quadratic case, the radial inverse of these constraints is not available in closed form in general.

5.3. Transmit power optimisation

Monotone optimisation arises naturally in wireless systems, as channel capacity is increasing in system resources such as transmit power, bandwidth, and antenna counts (Andrews et al., 2014). We consider the problem of minimising total transmit power subject to user-specific capacity requirements in a cellular downlink setting:

$$\min_{p \in [0,1]} \sum_{i=1}^n p_i, \quad \text{s.t. } C(p, s_j) \geq c_j, \quad j \in [m_g], \quad (5.2)$$

where p_i denotes the transmit power of the i -th radio transmitter, $s_j \in \mathbb{R}^3$ is the location of user j , and $C(p, s_j)$ denotes the channel capacity of user j . Since $C(p, s_j)$ is non-decreasing in p , (5.2) can be written in the canonical monotone form (2.1) via the substitution $y = 1 - p \in [0, 1]$:

$$\max_{y \in [0,1]} \sum_{i=1}^n y_i, \quad \text{s.t. } -C(1 - y, s_j) \leq -c_j, \quad j \in [m_g]. \quad (5.3)$$

If y^* solves (5.3), then $p^* = 1 - y^*$ solves (5.2).

Power optimisation typically relies on an accurate model of the capacity function $C(p, s_j)$. In modern networks, however, such models are difficult to obtain due to the increasing complexity of network dynamics and control mechanisms. Simplifying assumptions are typically required to produce tractable problems (see, e.g., (Georgiadis et al., 2006)).

Instead, we learn $C(p, s_j)$ from data, which may be obtained from system measurements or simulation. In our experiments we use the Cellular Radio Reference Model (CRRM) simulator (Briggs & Nur, 2025), which simulates radio links between a set of users and cell towers. Here, p_i is the transmit power of the i -th cell tower and $C(p, s_j)$ denotes the achievable capacity under a dynamically selected modulation and coding scheme for a user at s_j . Notably, the resulting capacity function $C(p, s_j)$ is piecewise constant in p and s_j , making local, gradient-based optimisation challenging.

We evaluate two variants of (5.3) corresponding to different signal path-loss models: (i) a power-law path-loss model, and (ii) the Urban Macrocell (UMa) model, which is more realistic and standards-compliant for urban deployments (3rd Generation Partnership Project (3GPP), 2025).

6. Numerical results

We evaluate the POA algorithm on the tasks described in Section 5, comparing performance under different learned representations of the monotone projection operator π_G . Specifically, we consider: (i) learning the constraint directly using relaxed certified monotone networks from Section 4.1 (M-Net) and computing projections using these learned constraints; (ii) learning radial-inverse surrogates using HM-RI from Section 4.2 and H-RI, M-RI, and RI from Section 4.3; and (iii) an oracle projection computed by bisection on the ground-truth constraint functions (ORACLE). As additional baselines, we include Sequential Least Squares Programming (SLSQP) (Kraft, 1988) and Constrained Optimization BY Linear Approximation (COBYLA) (Z. Zhang, 2023) from the `scipy.optimize` package (Virtanen et al., 2020). These are local constrained solvers that do not exploit monotonicity. We use them in a “learn-then-optimize” pipeline: we first fit constraint surrogates g_{θ_i} with non-monotone feed-forward networks, and then solve the resulting surrogate constrained problem with SLSQP/COBYLA. This tests whether exploiting monotonicity via POA and projection provides benefits beyond generic constrained optimisation on learned models. All non-oracle methods have access only to sampled constraint evaluations, whereas ORACLE assumes full access to the true constraint functions.

We set $n = 4$ for all problems, $m_g = 8$ for the quadratic and transmit power tasks, and $m_g = 2$ with $k = 8$ for multiplicative programming. Table 1 reports the *projected objective* value $f(\pi(x^*))$ for the returned solution x^* . Since all applications only impose lower-bound constraints (in addition to the box constraint $x \in [0, 1]$), the projection $\pi(x^*)$ is always feasible. Thus, $f(\pi(x^*))$ corresponds to the best feasible objective value along the ray $\{rx^* : r > 0\}$, providing a unified measure of solution quality across methods. We consider two data regimes: Limited, where models are trained on a fixed set of 512 samples, and Unlimited, where models are trained using an endless stream of randomly generated samples. In the limited regime, we report results only for radial inverse methods, as the other baselines were generally unreliable and often failed to produce meaningful solutions. For completeness, we report the unprojected objective values $f(x^*)$, the total constraint violation $\sum_i [g_i(x^*)]^+$, and algorithm run-time in Appendix E.1.

Table 1. Average projected objective (P-Obj.; higher is better) for each method, application, and data regime. Limited models are trained on a fixed set of 512 training samples while Unlimited models are trained using a stream of randomly generated samples (i.e., on-the-fly sampling rather than a fixed finite dataset). Results are averaged over 4000 randomly generated problem instances and five training seeds; uncertainties are small and omitted. ORACLE uses ground-truth constraints and is included only as a reference (not directly comparable). N/A denotes settings where the method consistently failed to converge or returned invalid/degenerate solutions, so P-Obj. is not meaningful.

Type	Method	Quadratic		Multiplicative		Power-law		UMa	
		Unlimited	Limited	Unlimited	Limited	Unlimited	Limited	Unlimited	Limited
Monotone	HM-RI	0.071	0.067	0.145	0.145	-1.20	-1.45	-1.34	-1.40
	M-RI	0.071	0.065	0.145	0.138	-1.14	-1.42	-1.32	-1.45
	H-RI	0.078	0.056	0.151	0.111	-0.95	-1.63	-1.02	-1.68
	RI	0.081	0.059	0.144	0.117	-1.03	-1.65	-1.09	-1.69
	M-Net	0.059	N/A	0.139	N/A	-1.16	N/A	-1.29	N/A
Local	SLSQP	0.074	N/A	0.142	N/A	-1.55	N/A	-1.62	N/A
	COBYLA	0.074	N/A	0.145	N/A	-1.75	N/A	-1.70	N/A
ORACLE		0.085	0.085	0.163	0.163	-0.57	-0.57	-0.75	-0.75

Accuracy. Table 1 shows that radial-inverse (RI) surrogates consistently achieve higher projected objective values than both M-Net and local baselines. This shows the advantage of leveraging monotonicity and supports the view that, within POA, learning the radial inverse is a more effective way to approximate the projection operator than learning the constraint function directly. In particular, RI models avoid the bisection search required by constraint-based projections, which is a major computational bottleneck in POA iterations. Compared to local optimisation methods, monotone approaches yield the largest gains on the transmit power problems, where piecewise-constant capacity constraints create large flat regions that are challenging for gradient-based solvers.

Generalisation under limited data. Comparing the two data regimes, we find that structured models, and monotone models in particular, are most beneficial when training data is scarce. As the dataset size decreases, explicitly enforcing monotonicity provides a strong inductive bias that improves generalisation. With abundant data, highly expressive unconstrained networks trained on monotone targets tend to exhibit approximately monotone behaviour even without explicit constraints, reducing the relative advantage of structured models. In this regime, the additional regularisation in (2.4) can degrade performance by diverting optimisation from the original training target.

Runtime. Table 2 reports runtime comparisons for a representative subset of methods in the unlimited-data regime. By eliminating the need for bisection, RI-based approaches are consistently faster than M-Net and, in some cases, even faster than ORACLE. Although RI remains slower than local search methods, this gap largely reflects the overhead of our current POA implementation and could likely be re-

duced with more optimised variants (see Appendix D.2).

Table 2. Mean runtime in seconds for selected methods on each application problem in the unlimited data regime. Uncertainties are small and omitted.

Method	Quad.	Mult.	Power-law	UMa
RI	0.91	1.85	0.31	0.39
M-Net	2.4	6.7	0.75	0.54
SLSQP	0.027	0.019	0.10	0.43
COBYLA	0.017	0.016	0.03	0.04
ORACLE	2.2	4.4	0.02	0.06

7. Conclusion

We presented a learning framework for integrating learned models into the POA algorithm for monotone optimisation. We argued that, within POA, it is more effective to learn the radial inverse—a core primitive for projection onto normal sets—than to approximate constraint functions directly. To enable this, we introduced the HM-RI architecture and provided sufficient structural conditions under which the learned map corresponds to the radial inverse of an increasing constraint, ensuring compatibility with POA.

Across four application settings, our experiments show that monotone optimisation with learned components achieves strong solution quality and consistently outperforms local constrained solvers on the evaluated tasks. Moreover, learning the radial inverse improves both runtime and projected objective relative to constraint-function surrogates, highlighting the value of aligning learned representations with the structure of the underlying optimisation algorithm. These results suggest radial-inverse learning as a promising direction for data-driven monotone optimisation.

References

Fajemisin, A. O., Maragno, D., & den Hertog, D. (2024). Optimization with constraint learning: A framework and survey. *European Journal of Operational Research*, 314(1), 1–14.

Jeon, Y., Lee, M., & Choi, J. Y. (2019). Neuro-optimization: Learning objective functions using neural networks. *arXiv preprint arXiv:1905.10079*.

Lin, J., Chen, Y., Zheng, H., Ding, M., Cheng, P., & Hanzo, L. (2021). A data-driven base station sleeping strategy based on traffic prediction. *IEEE Transactions on Network Science and Engineering*, 11(6), 5627–5643.

Hertrich, J., Wong, H. S., Denker, A., Ducotterd, S., Fang, Z., Haltmeier, M., Kereta, Ž., Kobler, E., Leong, O., Salehi, M. S., et al. (2025). Learning regularization functionals for inverse problems: A comparative study. *arXiv preprint arXiv:2510.01755*.

Zou, Z., Liu, J., Wohlberg, B., & Kamilov, U. S. (2023). Deep equilibrium learning of explicit regularization functionals for imaging inverse problems. *IEEE Open Journal of Signal Processing*, 4, 390–398.

Tong, J., Zhu, Y., Serra, T., & Burer, S. (2025). Optimization over trained neural networks: Going large with gradient-based algorithms. *arXiv preprint arXiv:2512.24295*.

Perakis, G., & Tsiorvas, A. (2022). Optimizing objective functions from trained relu neural networks via sampling. *arXiv preprint arXiv:2205.14189*.

Fischetti, M., & Jo, J. (2018). Deep neural networks and mixed integer linear optimization. *Constraints*, 23(3), 296–309.

Zhang, Y. J., Qian, L., & Huang, J. (2013). Monotonic optimization in communication and networking systems. *Foundations and Trends® in Networking*, 7(1), 1–75.

Golchi, S., Bingham, D. R., Chipman, H., & Campbell, D. A. (2015). Monotone emulation of computer experiments. *SIAM/ASA Journal on Uncertainty Quantification*, 3(1), 370–392.

Konno, H., Thach, P. T., & Tuy, H. (2013). *Optimization on low rank nonconvex structures* (Vol. 15). Springer Science & Business Media.

Tuy, H. (2000). Monotonic optimization: Problems and solution approaches. *SIAM Journal on Optimization*, 11(2), 464–494.

Jorswieck, E. A., & Larsson, E. G. (2010). Monotonic optimization framework for the two-user miso interference channel. *IEEE Transactions on Communications*, 58(7), 2159–2168.

Utschick, W., & Brehmer, J. (2011). Monotonic optimization framework for coordinated beamforming in multicell networks. *IEEE Transactions on Signal Processing*, 60(4), 1899–1909.

Tuy, H., Al-Khayyal, F., & Thach, P. T. (2005). Monotonic optimization: Branch and cut methods. In *Essays and surveys in global optimization* (pp. 39–78). Springer.

Fang, Z., Buchanan, S., & Sulam, J. (2024). What's in a prior? Learned proximal networks for inverse problems. *The Twelfth International Conference on Learning Representations*.

Beliakov, G. (2005). Monotonicity preserving approximation of multivariate scattered data. *BIT numerical mathematics*, 45(4), 653–677.

You, S., Ding, D., Canini, K., Pfeifer, J., & Gupta, M. (2017). Deep lattice networks and partial monotonic functions. *Advances in neural information processing systems*, 30.

Daniels, H., & Velikova, M. (2010). Monotone and partially monotone neural networks. *IEEE Transactions on Neural Networks*, 21(6), 906–917.

Runje, D., & Shankaranarayana, S. M. (2023). Constrained monotonic neural networks. *International Conference on Machine Learning*, 29338–29353.

Liu, X., Han, X., Zhang, N., & Liu, Q. (2020). Certified monotonic neural networks. *Advances in Neural Information Processing Systems*, 33, 15427–15438.

Schaefer, H. H., & Wolff, M. P. H. (1999). *Topological vector spaces* (2nd ed., Vol. 3). Springer New York. <https://doi.org/10.1007/978-1-4612-1468-7>

Bamberger, S., Heckel, R., & Krahmer, F. (2025). Approximating positive homogeneous functions with scale invariant neural networks. *Journal of Approximation Theory*, 106177.

Shorten, C., & Khoshgoftaar, T. M. (2019). A survey on image data augmentation for deep learning. *Journal of big data*, 6(1), 1–48.

Park, J., & Boyd, S. (2017). General heuristics for nonconvex quadratically constrained quadratic programming. *arXiv preprint arXiv:1703.07870*.

Tuy, H., & Luc, L. T. (2000). A new approach to optimization under monotonic constraint. *Journal of Global Optimization*, 18(1), 1–15.

Andrews, J. G., Singh, S., Ye, Q., Lin, X., & Dhillon, H. S. (2014). An overview of load balancing in hetnets: Old myths and open problems. *IEEE Wireless Communications*, 21(2), 18–25.

Georgiadis, L., Neely, M. J., & Tassiulas, L. (2006). *Resource allocation and cross-layer control in wireless networks*. Now Publishers Inc.

Briggs, K., & Nur, I. (2025). CRRM: A 5G system-level simulator. *arXiv preprint arXiv:2511.02692*.

3rd Generation Partnership Project (3GPP). (2025). *Study on channel model for frequencies from 0.5 to 100 ghz* (Technical Report No. TR 38.901) (Under change control; latest version for Release 19 as of 2025). 3GPP.

Kraft, D. (1988). A software package for sequential quadratic programming. *Forschungsbericht - Deutsche Forschungs- und Versuchsanstalt für Luft- und Raumfahrt*.

Zhang, Z. (2023). Prima: Reference implementation for powell's methods with modernization and amelioration.

Virtanen, P., Gommers, R., Oliphant, T. E., Haberland, M., Reddy, T., Cournapeau, D., Burovski, E., Peterson, P., Weckesser, W., Bright, J., van der Walt, S. J., Brett, M., Wilson, J., Millman, K. J., Mayorov, N., Nelson, A. R. J., Jones, E., Kern, R., Larson, E., ... SciPy 1.0 Contributors. (2020). SciPy 1.0: Fundamental Algorithms for Scientific Computing in Python. *Nature Methods*, 17, 261–272.

A. Proofs

A.1. Proof of radial inverse properties

Proof of Proposition 1. We demonstrate the four properties in order:

(Positive-homogenous in x) - For any $\alpha > 0$, $x \in \mathbb{R}_+^n$ and $y \in \mathbb{R}$, we have by the definition of ρ_g in (3.1):

$$\begin{aligned}\rho_g(\alpha x, y) &= \inf\{r > 0 : g(\alpha x/r) \leq y\} \\ &= \inf\{r > 0 : g(x/(r/\alpha)) \leq y\} \\ &= \alpha \rho_g(x, y).\end{aligned}$$

(Monotonicity) - We show monotonicity in x first. Let $x, x' \in \mathbb{R}_+^n$ with $x' \geq x$. Since g is increasing, we have $g(x'/r) \geq g(x/r)$ for any $r > 0$. Then,

$$\{r > 0 : g(x'/r) \leq y\} \subset \{r > 0 : g(x/r) \leq y\}$$

for any $y \in \mathbb{R}$. It follows that

$$\begin{aligned}\rho_g(x', y) &= \inf\{r > 0 : g(x'/r) \leq y\} \\ &\geq \inf\{r > 0 : g(x/r) \leq y\} = \rho_g(x, y).\end{aligned}$$

The monotonicity in y follows in a similar way: For $y, y' \in \mathbb{R}$ with $y \leq y'$ and all $x \in \mathbb{R}_+^n$, we have

$$\{r > 0 : g(x/r) \leq y\} \subset \{r > 0 : g(x/r) \leq y'\},$$

therefore

$$\begin{aligned}\rho_g(x, y) &= \inf\{r > 0 : g(x/r) \leq y\} \\ &\geq \inf\{r > 0 : g(x/r) \leq y'\} = \rho_g(x, y').\end{aligned}$$

(Right-continuity in y) - Fix $x \in \mathbb{R}_+^n$, $y \in \mathbb{R}$, and let $r = \rho_g(x, y)$. First, assume that $r \in [0, \infty)$. By the definition of ρ_g , for any $\delta > 0$ we have $x \notin (r - \delta)K(y)$. Further, the sublevel sets satisfy

$$K(y) = \bigcap_{\epsilon > 0} K(y + \epsilon). \quad (\text{A.1})$$

Hence, for any $\delta > 0$ there exists some $\epsilon > 0$ depending on δ such that for all $\epsilon' \in [0, \epsilon)$, we have

$$x \notin (r - \delta)K(y + \epsilon').$$

Using (3.2), we then compute

$$\begin{aligned}\rho_g(x, y + \epsilon') &= \gamma_{K(y + \epsilon')}(x) \\ &= \inf\{r > 0 : x \in rK(y + \epsilon')\} \\ &\geq r - \delta.\end{aligned}$$

As $r = \rho_g(x, y)$, the monotonicity of ρ_g in y implies $\rho_g(x, y + \epsilon') \leq r$, and hence

$$\rho_g(x, y + \epsilon') \in [r - \delta, r].$$

Since δ is arbitrary, this implies that continuity holds.

If $r = \infty$, then for any $M > 0$ we have $x \notin MK(y)$, and by (A.1) $x \notin MK(y + \epsilon)$ holds for all sufficiently small $\epsilon > 0$, implying $\rho_g(x, y + \epsilon) \geq M$; since M is arbitrary, $\rho_g(x, y + \epsilon) \rightarrow \infty$ as $\epsilon \rightarrow 0$.

(Well-posedness) - For all $x \in \mathbb{R}_+^n$, we have $x \in K(g(x))$ by the definition of K in Section 3.1. Therefore by (3.2)

$$\rho_g(x, g(x)) = \inf\{r > 0 : x \in rK(g(x))\} \leq 1.$$

Next, we show the lower-bound identity. By monotonicity, we observe that $g(0) \leq g(x)$ for all $x \in \mathbb{R}_+^n$ and hence there is no $x \in \mathbb{R}_+^n$ such that $g(x) \leq g(0) - 1$, implying

$$K(g(0) - 1) = \emptyset.$$

Therefore,

$$\rho_g(x, g(0) - 1) = \inf\{r > 0 : x \in r\emptyset\} = \infty,$$

implying $\rho_g(x, g(0) - 1) > 1$. We set $y = g(x)$ and $y' = g(0) - 1$, and it follows that $y > y'$ and (3.3) holds.

□

A.2. Proof of projections as radial inverse functions

In this section, we provide the proofs of Proposition 2 and Proposition 3.

Proof of Proposition 2. Recall the definition (Section 2.2) of monotone projection onto a normal set:

$$\pi_{\mathcal{G}}(x) = \alpha_{\mathcal{G}}(x)x, \quad \alpha_{\mathcal{G}}(x) = \sup\{\alpha > 0 : \alpha x \in \mathcal{G}\},$$

and the gauge function:

$$\gamma_S(x) = \inf\{r > 0 : x \in rS\}, \quad S \subset \mathbb{R}_+^n.$$

If we accept $0^{-1} = \infty$, we have the identity $\alpha_S(x) = (\gamma_S(x))^{-1}$, for any set $S \subset \mathbb{R}_+^n$. However, note that by the compactness of \mathcal{G} , it follows that $\gamma_{\mathcal{G}}(x) > 0$ for all $x \in \mathbb{R}_+^n$ – since otherwise $\{rx : r > 0\} \subset \mathcal{G}$. This ensures the division-by-zero case does not occur with \mathcal{G} .

For the normal set \mathcal{G} , we compute

$$\begin{aligned} \alpha_{\mathcal{G}}(x) &= \sup\{\alpha > 0 : g_i(\alpha x) \leq u_i, i \in [m_g]\} \\ &= \sup\{\alpha > 0 : \max_{i \in [m_g]}(g_i(\alpha x) - u_i) \leq 0\} \\ &= \min_{i \in [m_g]}(\sup\{\alpha > 0 : g_i(\alpha x) - u_i \leq 0\}) \\ &= \min_{i \in [m_g]} \alpha_{\mathcal{G}_i}(x), \end{aligned}$$

where

$$\mathcal{G}_i = \{x \in \mathbb{R}_+^n : g_i(x) \leq u_i\}.$$

The radial inverse satisfies $\rho_{g_i}(x, u_i) = \gamma_{\mathcal{G}_i}(x)$. This yields:

$$\begin{aligned} \pi_{\mathcal{G}}(x) &= \alpha_{\mathcal{G}}(x)x \\ &= (\min_{i \in [m_g]} \alpha_{\mathcal{G}_i}(x)) x \\ &= (\min_{i \in [m_g]} [\gamma_{\mathcal{G}_i}(x)]^{-1}) x \\ &= (\min_{i \in [m_g]} [\rho_{g_i}(x, u_i)]^{-1}) x \\ &= \left(\max_{i \in [m_g]} \rho_{g_i}(x, u_i) \right)^{-1} x. \end{aligned}$$

□

Proof of Proposition 3. First, we show that positive-homogeneity implies that h is a gauge function:

$$\begin{aligned} h(x, y) &= \inf\{r > 0 : h(x, y) \leq r\} \\ &= \inf\{r > 0 : h\left(\frac{x}{r}, y\right) \leq 1\} \\ &= \inf\{r > 0 : x \in rK(y)\} \\ &= \gamma_{K(y)}(x) \end{aligned}$$

where

$$K(y) = \{z \in \mathbb{R}_+^n : h(z, y) \leq 1\}.$$

By y -monotonicity of h , these sets are nested – meaning that for $y' \geq y$ we have

$$K(y) \subset K(y').$$

We then show that $K(y)$ are the sub-level sets of a function g , which we define as:

$$g(x) := \inf\{y \in \mathbb{R} : x \in K(y)\}.$$

The well-posedness property of h ensures that, for each $x \in \mathbb{R}_+^n$, there exists $y_1, y_2 \in \mathbb{R}_+^n$ such that

$$x \in K(y_1), \quad \text{and} \quad x \notin K(y_2).$$

This, along with the fact that the sets $K(y)$ are nested, implies that $\{y \in \mathbb{R} : x \in K(y)\}$ is non-empty and bounded from below for all x , ensuring that g is always finite-valued. Using the right-continuity of h , we show that $K(y)$ are precisely the sub-level sets of g

$$\begin{aligned} g(x) \leq y &\iff x \in \bigcap_{\epsilon > 0} K(y + \epsilon) \\ &\iff h(x, y + \epsilon) \leq 1, \quad \forall \epsilon > 0 \\ &\iff h(x, y) \leq 1 \\ &\iff x \in K(y). \end{aligned}$$

It remains to show that g is increasing, which follows from x -monotonicity of h . Let $x' \geq x$, then

$$1 \geq h(x', g(x')) \geq h(x, g(x'))$$

therefore $x \in K(g(x'))$ and $g(x) \leq g(x')$. \square

Well-posedness assumption. We note that the well-posedness assumption is used solely to ensure that the resulting function g has finite values. The remainder of the argument does not rely on this property. If we instead accept $\inf \mathbb{R} = -\infty$ and permit g to take values in $\{-\infty, \infty\}$, the assumption can be dropped. Under this interpretation, even when ϕ fails to satisfy well-posedness, it still corresponds to a valid radial inverse.

B. Polyblock Outer Approximation (POA) details

B.1. Bisection search

In POA, we only compute monotone projections for $x \notin \mathcal{G}$, where we have $r_{\mathcal{G}}(x) \in [0, 1)$. Therefore, for computing projections, it is sufficient check where the line segment $\{rx : r \in [0, 1)\}$ intersects the boundary of \mathcal{G} . This is done by performing a line-search to find zeros of the monotone function $g'(x) := \max_i(g_i(x) - u_i)$. We include psudocode in Algorithm 2. If constraint function g_i is strictly monotone, then it is possible to replace the *while* condition with $\|g'(rx)\| > \epsilon$, and return r instead.

B.2. Vertex refinement

The polyblocks V^t are refined by cutting out the cone (z^t, ∞) at each iteration. The remaining set is a polyblock defined by the vertices

$$\hat{V}^{t+1} = (V^t / (z^t, \infty)) \cup W^t,$$

where

$$W^t = \{s - (s_i - z_i^t) e_i : s \in V^t, s > z^t, i \in [n]\},$$

and e_i is the i 'th basis unit vector. It can be seen that

$$P_{\hat{V}^{t+1}} = P_{V^t} / (z_t, \infty).$$

Since the $\mathcal{H}^c = P_{\mathcal{H}^c}$, we can also remove infeasible vertices from \hat{V}^{t+1} removing any elements from \mathcal{F} :

$$V^{t+1} = \hat{V}^{t+1} \cap \mathcal{H}. \quad (\text{B.1})$$

B.3. Convergence

This vertex refinement process continues until the stopping condition

$$\max_{s \leq t, z^s \in \mathcal{H}} f(z^s) + \epsilon \geq \max_{x \in V^t} f(x)$$

Algorithm 1 The Polyblock Outer Approximation algorithm

Inputs: $f, \pi_{\mathcal{G}}, \mathcal{H}, b, \epsilon$
Output: \hat{z}

```

 $V \leftarrow \{b\}$ 
 $\hat{x} \leftarrow b$ 
 $f_{\text{best}} \leftarrow -\infty$ 
while  $f_{\text{best}} + \epsilon < f(x^*)$  do
     $z \leftarrow \pi_{\mathcal{G}}(\hat{x})$ 
    if  $f(z) > f_{\text{best}}$  and  $z \in \mathcal{H}$  then
         $\hat{z} \leftarrow z$ 
         $f_{\text{best}} \leftarrow f(z)$ 
    end if
     $V \leftarrow \text{Update as (B.1)}$ 
     $\hat{x} \leftarrow \arg \max_{x \in V} f(x)$ 
end while

```

is met for a given tolerance $\epsilon > 0$. If the algorithm terminates in finitely many iterations, then z^s is ϵ -optimal. Otherwise, if the algorithm is infinite, it can still be shown to converge to an optimal solution under mild conditions.

Theorem 1. Assume that f is upper-continuous and $\mathcal{G} \cap \mathcal{H} \subset \mathbb{R}_{++}^n$. If Algorithm 1 is infinite, then the sequences $\{\hat{x}^t\}, \{z^t\}$ contain subsequences converging to a solution of (2.1).

See (Tuy, 2000) for a proof and a more extensive discussion of the algorithm.

B.4. Origin shift

One of the assumptions of Theorem 1 is that feasible set doesn't intersect the coordinate axis. We show that this assumption is not restrictive and can always be achieved by a variable transformation. If this does not hold for a given problem, it is possible to shift the origin as follows. For $\alpha > 0$, define

$$\begin{aligned} f'(x) &:= f(x - \alpha), \\ \mathcal{G}' &:= (\alpha + \mathcal{G} - \mathbb{R}_+^n) \cap \mathbb{R}_+^n, \\ \mathcal{H}' &:= \alpha + \mathcal{H}. \end{aligned}$$

It can be seen that the problem

$$\max_x f'(x), \text{ s.t. } x \in \mathcal{G}' \cap \mathcal{H}' \quad (\text{B.2})$$

is monotone, satisfies the required assumption, and is equivalent to the original problem in the sense that if y^* solves (B.2), then $x^* = y^* - \alpha$ solves the original problem.

B.5. Vertex reduction

The size of the vertex sets V^t tends to grow exponentially with t , which can cause memory issues. We describe some

methods to reduce their size.

Given the current best solution

$$\hat{z}^t = \arg \max_{s < t, x_s \in \mathcal{H}} f(z^t),$$

it is sufficient to search only for solutions better than \hat{z}^t . Therefore, we can remove all $x \in \hat{V}^{t+1}$ for which $f(x) + \epsilon < f(\hat{z}^t)$. Moreover, there are some redundant vertices $x \in \hat{V}^{t+1}$ which are dominated by some other vertex $y \geq x$ with $y \in \hat{V}^{t+1}$. To avoid this, we compute the set W^t of added vertices in such a way that no new vertex lies in the rectangular set of any of the removed vertices $V^t/(z^t, \infty)$. More specifically we take

$$W^t = \{s^{(i)} \notin V^t / \{s\} : s \in V^t, s > z^t, i \in [n]\},$$

where $s^{(i)} = s - (s_i - z_i^t)e_i$. This removes all redundant vertices from V^t .

To place a hard limit on the vertex-set size, we can restart the algorithm when a vertex limit V_{\max} is exceeded. Specifically, if $|V^t| > V_{\max}$, we set $V^t \leftarrow \{b\}$ after computing z^t and before the update in (B.1).

C. Certified monotone networks

In this appendix, we describe the monotone certification method and our two proposed relaxations in more detail.

C.1. Verifying monotonicity

The original certified monotone method relies on verifying the monotonicity of two-layer networks with ReLU activations by formulating the gradients of such networks as a system of mixed-integer equations. More specifically, we define a two-layer network with a scalar output

$$g(x) = \sum_{j \in [w]} a_j (w_j^T x + b_j)^+,$$

where the final bias is omitted as it does not affect monotonicity. The gradient of g is

$$\nabla g(x) = \sum_{j \in [w]} z_j \alpha_j w_j,$$

where each $z_j = \mathbb{1}_{w_j^T x + b_j \geq 0}$ is the activation state of neuron j . Assuming the input is bounded, which holds in our application with $x \in P_b$, there exists $l_j, u_j \in \mathbb{R}$ such that the first affine layer is bounded as

$$l_j \leq w_j^T x + b_j \leq u_j, \quad j \in [w]$$

The activations z_j may then be written as a set of linear constraints:

$$z_j \in S_j(x),$$

where

$$S_j(x) := \{z' \in \{0, 1\} : l_j(1 - z') \leq w_j^T x + b_j \leq u_j z'\},$$

it can be seen that $|S_j(x)| \equiv 1$. The network g_θ is monotone iff

$$\nabla g(x)_i \geq 0, \quad \text{for all } x \in P_a, i \in [n]. \quad (\text{C.1})$$

To confirm this, we solve the MILP:

$$\min_{\substack{x \in P_b \\ v \in \mathbb{R}_+^n}} \sum_j (z_j \alpha_j w_j)^T v, \quad \text{s.t. } z_j \in S_j(x), \|v\|_1 = 1, \quad (\text{C.2})$$

which yields the minimum value of $\nabla g(x)_i$ for checking (C.1).

In practice, we do not need to solve the MILP exactly. To speed up the verification process, it is sufficient to satisfy at least one of two stopping conditions: either finding a counter-example to (C.1), or a non-negative bound lower on the objective $\nabla g(x)_i$. Branch-and-bound algorithms used for solving MILPs can naturally reach either condition before solving (C.2) exactly.

We note that this method can be expanded to enforce monotonicity on only a subset of components of x .

C.2. δ -relaxation

The δ -relaxation described in Section 4.1 is implemented by simply replacing condition (C.1) by

$$\nabla g(x)_i \geq \delta, \quad \text{for all } x \in P_a, i \in [n], \quad (\text{C.3})$$

where we set $\delta = -0.1$ in our experiments. The MILP stopping conditions are adjusted accordingly.

C.3. τ -relaxation

The τ -relaxation enforces monotonicity on only larger affine pieces of g . More specifically, we enforce (C.3) only for $x \in P_b$ for which the neuron activations z are fixed at all perturbed points $x + v$ for all $v \in \mathbb{R}^n$ with $\|v\|_\infty \leq \tau$. To verify this condition, it is sufficient to replace S_j in (C.2) with the set

$$S'_j(x) = \left\{ z' \in \{0, 1\} : \begin{array}{l} w_j^T x + b_j + \tau'_j \leq u_j z', \\ w_j^T x + b_j - \tau'_j \geq l_j(1 - z') \end{array} \right\},$$

where

$$\tau'_j = \max\{w_j^T v : \|v\|_\infty \leq \tau\} = \tau \|w_j\|_1.$$

In our experiments, we set $\tau = 0.01$.

D. Experimental details

D.1. Hardware

All experiments were conducted on a single machine with an NVIDIA GeForce RTX 4090 GPU and an AMD Ryzen 9 7950X3D CPU.

D.2. POA implementation

For the POA algorithm, We used a numerical tolerance of $\epsilon = 1e-3$ and a maximum vertex size $V_{\max} = 10,000$. Where applicable, we used a tolerance of $\epsilon = 1e-4$ for the bisection search.

We used a simple implementation of POA in Python, prioritising clarity over efficiency. To simplify the implementation, both \hat{x}^t and the vertex set V^t were computed using operations on unstructured arrays. Since the vertex set is updated iteratively, more efficient data structures could be employed, such as maintaining sorted arrays of vertex objective values and coordinate values. This would allow \hat{x}^t and V^t to be updated more efficiently and would uniformly reduce the runtimes reported in Table 1.

Algorithm 2 The bisection search algorithm used for computing monotone projections

```

Inputs:  $\{g_i\}_{i \in [m_g]}, x, \epsilon$ ,
Output:  $r_{\min} x$ 
 $(r_{\max}, r_{\min}, r) \leftarrow (1, 0, 0.5)$ 
 $g'(x) := \max_i(g_i(x) - u_i)$ 
while  $r_{\max} - r_{\min} > \epsilon$  do
    if  $g'(rx) > 0$  then
         $r_{\max} \leftarrow r$ 
    else
         $r_{\min} \leftarrow r$ 
    end if
     $r \leftarrow (r_{\max} + r_{\min})/2$ 
end while

```

D.3. MILP solver

We used the paid version of Gurobi to solve the certification MILP in (C.2). We set the **MIPFOCUS** parameter to 2 (targets optimality), and the **CUTS** parameter to 3 (very aggressive). We used 32 threads and set a 5 minute time limit was set for the solver, after which the model was flagged as uncertified.

D.4. Model design

All radial inverse models considered had an identical architecture for each application considered. σ_θ and ψ_θ had six layers (three sets of two-layer monotone networks) with 64 neurons each. M-Net and the feed-forward models used

for testing SLSQP had six layers, alternating with 100 and 64 neurons. Both types of model had an approximately equal number of learned parameters. For the relaxed monotonicity experiments in Appendix E.2, models sizes were reduced to only two layers.

D.5. Training

All models were trained using Adam with a learning rate of $2e-4$ and a batch size of 512. Monotone networks were trained for an initial 4000 iterations, then 1000 iterations for each training loop reset before model certification (as described in Appendix C). The regularisation factor was initialized at $c = 0.05$ and increased by a factor of 1.2 (1.5 for the transmit power problem) after each reset, up to a maximum of 0.2 (or 1.0, respectively).

Models with no monotone networks were trained for 20 000 iterations. This choice was made to balance the training time for each type of model.

D.6. Problem generation

For each class of problems considered in Section 5, we reported results on sets of 4000 randomly generated problem instances. For the problems in Sections 5.1 and 5.2, elements of the linear and quadratic parameters, c_i and Q_i , were sampled uniformly from $[0, 1]$. For the communication problem in Section 5.3, instances were generated automatically using the CRRM simulator (Briggs & Nur, 2025). In all cases, the constraint targets u_i were obtained by evaluating each constraint at a randomly chosen point $x \in [0, 0.5]$, ensuring that all generated constraints are feasible.

E. Additional results

This appendix provides additional quantitative results complementing the main experiments in Section 6.

E.1. Unprojected objective and constraint violation

Table 3 reports the objective value and constraint violation of the *unprojected* solutions returned by each method, along with its algorithm runtimes.

Recall that our algorithms return a candidate solution $x^* \in [0, 1]$, which may not be feasible under the true constraints. To compare methods in a consistent way, the main paper evaluates solutions using the *projected objective* $f(\pi_G(x^*))$, which corresponds to the best feasible point obtained by projecting x^* along its ray. In contrast, Table 3 reports the raw (unprojected) objective $f(x^*)$ together with the total constraint violation $\text{viol}(x^*) := \sum_{i=1}^{m_g} [g_i(x^*)]^+$. Lower violation indicates greater feasibility, but a method may achieve a higher objective only

Table 3. Average unprojected objective (Obj.) $f(x^*)$, total constraint violation (Viol.) $\sum_i [g_i(x^*)]^+$, and runtime (in seconds) for each method and application in both the limited and unlimited data scenarios. All tasks are maximisation problems, so higher objective values are preferable, while lower violation indicates better feasibility, resulting in a trade off between objective and violation. Results are averaged over 4000 randomly generated problem instances and five training seeds (uncertainties are small and omitted).

Data	Method	Quadratic			Multiplicative			Power-law			UMa		
		Obj.	Viol.	Time	Obj.	Viol.	Time	Obj.	Viol.	Time	Obj.	Viol.	Time
L	HM-RI	0.141	0.21	1.38	0.253	0.116	1.92	-1.68	0.27	1.98	-1.52	0.31	1.29
	M-RI	0.198	0.43	1.76	0.323	0.218	2.08	-1.63	0.25	0.53	-1.59	0.27	0.39
	H-RI	0.213	0.66	1.96	0.281	0.253	2.25	-1.45	0.88	0.06	-1.46	1.49	0.06
	RI	0.179	0.41	1.95	0.275	0.217	2.25	-1.52	0.86	0.07	-1.61	0.81	0.09
U	HM-RI	0.096	0.059	1.13	0.176	0.043	1.61	-0.90	0.84	2.15	-1.28	0.60	2.10
	M-RI	0.094	0.051	0.90	0.142	0.016	1.15	-1.23	0.30	0.42	-1.24	0.46	0.18
	H-RI	0.104	0.044	1.15	0.228	0.073	1.97	-0.93	0.34	0.56	-1.08	0.24	0.34
	RI	0.098	0.031	0.91	0.225	0.081	1.85	-1.22	0.12	0.31	-1.30	0.12	0.39
	M-Net	0.052	0.011	2.4	0.129	0.043	6.7	-0.28	1.56	0.75	-1.74	0.20	0.54
	SLSQP	0.087	0.060	0.027	0.164	0.054	0.019	-0.90	3.03	0.10	-1.72	0.30	0.43
	COBYLA	0.083	0.020	0.017	0.161	0.049	0.016	-0.28	1.56	0.03	-1.39	1.67	0.04

by violating constraints more strongly, so these numbers should be interpreted jointly.

Overall, in the unlimited data regime, the radial-inverse (RI) methods achieve high unprojected objective values. Among them, H-RI attains the largest objective on all tasks except the power-law setting, where HM-RI is marginally higher. Compared to the local baselines, H-RI yields smaller constraint violation on two of the four tasks (power-law and UMa), while achieving competitive objectives.

For the power-law task, H-RI attains a lower unprojected objective than SLSQP/COBYLA, but its constraint violation is substantially smaller (0.34 vs. 3.03 and 1.56, respectively). After projection, this leads to the best projected objective (Table 1). Conversely, for the multiplicative problem, H-RI incurs higher violation than the local baselines (0.073 vs. 0.054/0.049) but achieves a markedly larger objective (0.228 vs. 0.164/0.161), again yielding the strongest projected objective after projection (Table 1).

As expected, solution quality is uniformly reduced in the limited data regime. Monotone radial inverse networks (HM-RI and M-RI) are seen to have the highest quality solutions in this regime, as indicated by their projected objectives in Table 1.

E.2. Relaxed monotonicity results

To assess the two monotonicity relaxations from Section 4.1, we report test losses and the number of training-loop restarts when learning channel capacity models for the UMa task (Section 5.3). We ablate each relaxation by setting either (or both) of δ and τ to zero. As shown in Table 4, setting $\tau > 0$ consistently reduces the number of restarts across both values of δ , improving training stabil-

Table 4. Mean test loss and number of training-loop restarts for monotonicity relaxation ablations on the UMa task, averaged over five training seeds.

δ	τ	Loss	Restarts
-0.1	0.01	0.103 ± 0.004	13.0 ± 0.4
0.0	0.01	0.5 ± 0.1	23 ± 1
-0.1	0.0	0.080 ± 0.002	29 ± 3
0.0	0.0	0.70 ± 0.06	26 ± 1

ity. In contrast, $\delta < 0$ primarily improves predictive performance, reducing test loss by nearly an order of magnitude. Overall, δ provides the main accuracy gains, whereas τ improves optimisation robustness under strict monotonicity constraints. The differences in test loss between configurations with and without τ at $\delta = -0.1$ are largely explained by restart overhead (and hence differences in effective training time), rather than a detrimental effect of τ , which is consistent with the remaining ablations.